ELSEVIER

Journal of Non-Crystalline Solids 185 (1995) 41–48

JOURNAL OF NON-CRYSTALLINE SOLIDS

Structural evolution of a porous type-VI sol–gel silica glass

F.G. Araújo, G.P. LaTorre, L.L. Hench *

University of Florida, Advanced Materials Research Center, One Progress Blvd., #14, Alachua, FL 32615, USA

Received 18 January 1994; revised manuscript received 29 September 1994

Abstract

The structural evolution of type-VI porous sol–gel-derived optical glasses is described. The average pore radius of the glasses studied is 30 Å, with an exceptionally narrow pore size distribution. These glasses are particularly suited to laser surface densification. Their properties make them also attractive as matrices for impregnation of second phases and as a substrate material for the production of fully dense optical lens elements and micro-optical devices. The properties of the matrices are reported for the as-dried state to densities approaching 2.2 g/cm^3, with thermal treatments from room temperature to 1060°C. The parameters of sintering for the gel–glass transformation are measured, and the phenomena occurring for three temperature ranges are evaluated. An activation energy of 65 ± 9 kcal/mol for sintering with a structure factor $n = 1.0 \pm 0.3$ was found for the initial stage sintering of the material.

1. Introduction

A new generation of porous type-VI gel–silica glasses [1,2] has been developed which have improved optical and structural properties, as well as high production yields [3,4]. Monoliths with pore radii ranging from 16 to 30 Å were produced. This paper describes the structural evolution as a function of thermal treatment for the 30 Å gels only, which have had properties reported previously [3,4].

The motivation for developing this new generation of gel–silica matrices, was the need for a porous pure silica–gel monolith suited for surface laser densification of optical channel waveguides [4], as well as for the impregnation of optically active organic molecules [5–7]. For these applications the requirements are high optical transparency, good surface quality, improved mechanical characteristics and increased pore volumes. All of these requirements have been achieved for this new generation of gels, when compared with previous systems [1,3]. A high degree of homogeneity of the pore structure allows the densification of these materials without chlorination [2].

Changes in the physical properties and the structure of the 30 Å gels with temperature were followed with dilatometry. Densification of the material was analyzed using a constant-heating-rate technique, in an attempt to reproduce the actual processing of the optical monoliths, and to overcome the limitations of isothermal analyses. The densification of the gels could be divided into three regions according to shrinkage rates, and the mechanisms taking place in each of the regions is outlined. For the highest processing temperatures classical sintering was found to occur, and the activation energy was calculated.

* Corresponding author. Tel: +1-904 462 5445. Telefax: +1-904 462 5470.

0022-3093/95/$09.50
SSDI 0022-3093(94)00653-9

The results are compared with previous works on multicomponent sol–gel-derived glasses [8].

The densification of some alkoxide-derived sol–gel glass systems has been extensively studied by other authors [8], and the results generalized for any silica-based glass derived by the same method [8]. However, the densification of gels is directly related to the behavior of their viscosity with increasing temperature, which is strongly dependent on both the chemical composition and the water content of the glass [9–14]. As the chemical composition of a sol–gel-based silica glass is a major variable from system to system, the generalization of the results found for one type of system becomes a difficult task.

2. Experimental

Monoliths of the 30 Å type-VI pure silica glasses were prepared from the acid catalysis of tetramethylorthosilicate (TMOS), as described earlier [1,2]. Samples of the gel were densified in a box furnace at different temperatures and times in ambient air, being subsequently analyzed for their pore structure by nitrogen adsorption, using a nitrogen adsorption/desorption system (Autosorb 6, Quantachrome Corporation). Helium pycnometry in a micropycnometer (Quantachrome) was performed for all samples to follow the evolution of the structural density of the silica network with temperature. UV–VIS analysis in a spectrometer (Perkin–Elmer Lambda 9) and (FTIR) analysis in a spectrometer (Nicolet 20 SXB) were done for all samples (triplicates were produced), and typical spectra are shown. Thermogravimetric analysis in a thermal analyzer system (DuPont 1090) and dilatometry in a dilatomer (Theta Dilatronic) were performed on dried gels in ambient air in conditions close to those used in the production of the densified monoliths themselves. Dilatometry was performed in helium and oxygen atmospheres.

3. Physical characterization during densification

Dilatometry on 30 Å gels densified at constant heating rates to approximately 1060°C reveals three densification regions (Fig. 1). The dilatometry curve

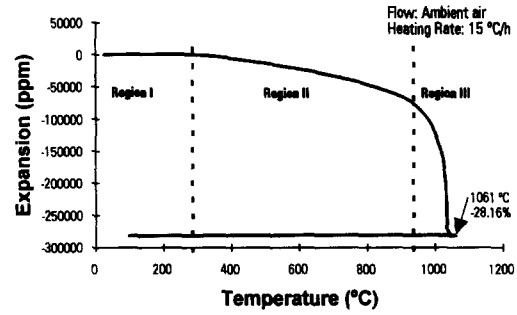

Fig. 1. Dilatometry curve of a 30 Å porous silica glass, densified at a heating rate of 15°C/h in ambient air. The densification curve is divided into three regions, according to the densification rate.

in Fig. 1 was obtained for a heating rate of 15°C/h, but the same features were observed for rates of 12 and 21°C/h. A total linear shrinkage of −28.16% was observed, leading to a final bulk density close to 2.1 g/cm^3. This corresponds to more than 95% densification at temperatures as low as 1060°C.

The densification behavior shown in Fig. 1 is described as a first region of 'constant volume' from room temperature up to 300°C, a second region of 'slow shrinkage' between 300 and 950°C and a third region of 'fast shrinkage' above 950°C. The total linear shrinkage achieved at the maximum temperature of the densification schedule was of −28.54% for the sample densified at a heating rate of 12°C/h, and of −26.78% for the sample densified at a heating rate of 21°C/h. The faster the heating rate, the smaller is the total shrinkage. However, samples densified at heating rates faster than 21°C/h become distorted, owing to the thermal stresses induced, while heating rates slower than 12°C/h are impractical. A heating rate of 15°C/h was chosen for the studies.

The pore volume from nitrogen adsorption analysis on samples of the 30 Å porous silica matrices densified at different temperatures for various isothermal holding times (0–5 h) is shown in Fig. 2. The same trend observed for the linear expansion is observed for the structural properties of the matrices, e.g., a first slow 'decrease' followed by a fast decrease in value for the higher temperatures. The surface area and the pore radius present curves similar to the pore volume curve. These properties are more sensitive to the densification temperature than to the isothermal holding time. The nitrogen adsorp-

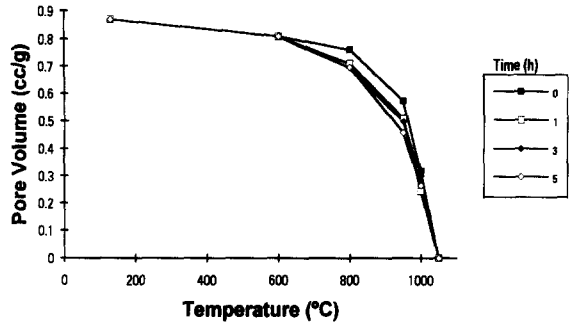

Fig. 2. Evolution of the pore volume of the 30 Å porous silica glasses with temperature and time, as measured by nitrogen adsorption.

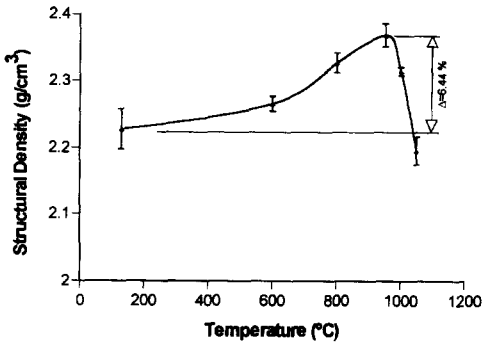

Fig. 4. Structural density of 30 Å porous silica glasses at different temperatures, measured by helium pycnometry.

tion/desorption isotherms, and the pore size distributions of the 30 Å porous silica matrices treated at different temperatures, presented in a previous work [3], show that the nature of the pores does not change with temperature, and according to de Boer [15,16] the porous network can be molded by cylindrical pores open at both ends.

The pore radius distribution shown in Fig. 3 becomes narrower as the temperature increases. The pore size distribution plays an important role both in the optical properties [17] and in the densification properties of the gel [18–20]. A narrow pore radius distribution produces a narrow optical loss due to low Rayleigh scattering, enabling the porous matrix to be used as an optical material. A narrow pore radius distribution also induces a faster densification [18,20]. The larger pores tend to shrink more slowly than the smaller pores, so that the larger pores are subjected to compressive stresses by the smaller pores, while the smaller pores are subjected to tensile

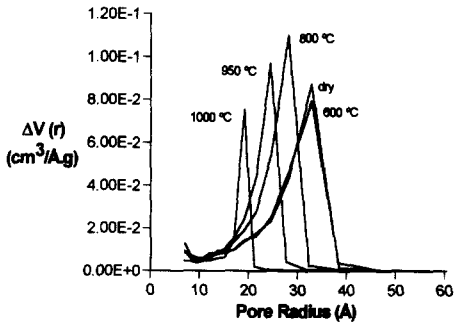

Fig. 3. Nitrogen adsorption pore size distribution of the 30 Å porous silica glasses treated at different temperatures.

stresses by the larger pores [20]. Therefore the densification rates of both sets of pores are affected by the pore size distribution.

Fig. 4 shows the evolution of the structural density of the 30 Å type-VI gel–glasses with the treatment temperature, as measured by a helium pycnometer. The structural density of the gels increases about 6.4% from the as-dried sample to the sample treated at 950°C, with a maximum value of 2.37 g/cm^3. The initial increase in the structural density (below 600°C) has a strong component due to the weight loss by the material during heating, as the thermogravimetric analysis (TGA) results suggest. A structural density of 2.27 g/cm^3 is larger than the melt glass density, which can be explained by a structure more free of defects, as is expected for a sol–gel-derived glass [20]. Indices of refraction reported by Hench et al. [1] that are larger than the indices of fused silicas are consistent with this result. The maximum in the structural density at 950°C is a result of a maximum number of three-member rings of silicate tetrahedra measured by Raman spectroscopy [2,31] together with the beginning of pore closure, when part of the porosity ceases being accessible to the adsorbate molecules.

Fig. 5 shows IR reflectance spectra of 30 Å type-VI porous glasses densified at different temperatures, as measured by a FTIR microspectrometer. For the samples densified at higher temperatures, the position of the peak maximum, PP, is shifted to higher values. The maximum value of PP at 1123.3 cm^{-1} is attributed to the Si–O–Si asymmetric stretching vibrational mode [21]. The shift in the

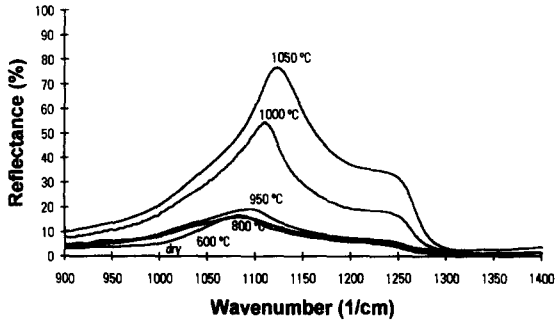

Fig. 5. FTIR spectra of 30 Å porous silica glasses at different temperatures, showing the Si–O–Si stretching vibration absorption peak.

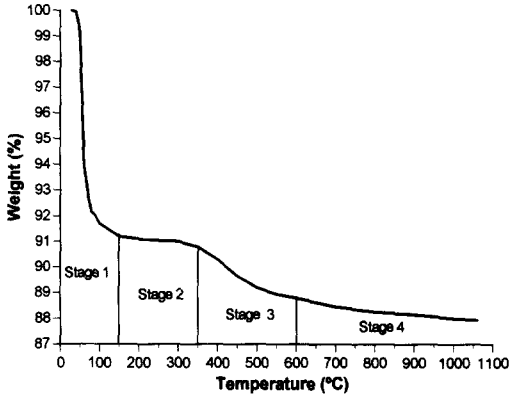

Fig. 6. Weight loss of a 30 Å porous silica glass heated at 0.3°C/min in ambient air, measured by TGA.

peak to higher wave numbers with an increase in processing temperature is a measure of the densification of the material [4,22]. Chia et al. have reported a PP at 1122 cm^{-1} for a fully dense pure commercial optical silica [23]. A PP at 1123.3 cm^{-1} for the 30 Å type-VI matrices indicates that, at least at its surface, this material reaches a density higher than the melt glass density, confirming the results from the helium pycnometer. UV–VIS spectra show absorption bands for the sample treated at 1050°C, which indicate that chemical water in the form of silanol groups, Si–OH, is present in the system.

Fig. 6 shows the result of a TGA performed on a 30 Å type-VI porous glass initially as dried, at a constant heating rate of 18°C/h. The TGA curve can be roughly divided into four stages. In stage 1 there is a sharp decrease in the weight of the sample when it is heated from room temperature up to about 150°C, accounting for a weight loss of approximately 8.75%. Stage 2 comprises a very slow weight loss between 150 and 350°C, with a weight loss around 0.25%. Stage 3 occurs between 350 and 600°C, with a weight loss of 2.25%. Stage 4 occurs from 600°C up to 1060°C and corresponds to a very slow weight loss of about 0.75%.

Stage 1 corresponds to the loss of physical water [24]. The weight loss in stages 2, 3 and 4 is associated both with the removal of the organic groups by oxidation and with evaporation of water formed from polycondensation reactions [8]. The shape of the curve suggests though that stages 2 and 4 correspond mainly to polycondensation, as they present similar weight loss rates. Stage 3 consists of a combination of elimination of organic groups and polycondensation. Table 1 shows the weight loss, the weight loss rate, the estimated water loss and the percentage of the siloxane bonds on the sample formed by poly-

Table 1
Siloxane bonds formed during densification of a 30 Å porous silica glass

Weight loss stage	Weight loss (%)	Weight loss rate ($\times 10^{-3}$ %/°C)	Estimated [a] water loss ($\times 10^{-3}$ mol/g)	Formed ≡Si–O–Si≡ bonds (%) [b]
1	8.75	58.330	4.86	– [c]
2	0.25	1.250	0.14	0.079
3	2.25	9.000	1.25 [d]	0.720
4	0.75	1.875	0.41	0.237
Total	12.00	–	6.66	1.036

[a] Calculated from the sample weight.
[b] Calculated from the average number of TMOS molecules initially present on the sample and from the water loss in the stage.
[c] The water loss in this stage is associated with physical water.
[d] As a portion of the organic groups eliminated in stage 3 are bonded to silicon tetrahedra terminations, they are approximated by lost water, in order to calculate the number of siloxane bonds formed.

condensation during densification as calculated from the water loss in each stage. As a portion of the organic groups eliminated in stage 3 is bonded to silicon tetrahedra terminations, they are approximated by lost water, in order to calculate the number of siloxane bonds formed. The samples are dried prior to densification in the range of temperatures of stage 1, thus the water lost corresponds to physical water (the weight loss seen in the curve in this stage is the water that the sample adsorbs inside the TGA furnace). Therefore, a maximum of 1.036% of polycondensation is estimated to occur during densification.

4. Densification mechanisms

4.1. Region I

The first region of densification shown in Fig. 1 and described as a constant volume region, instead of having a constant volume as may appear, actually shows a 1000 ppm positive expansion experienced by the dried 30 Å monolith, as can be seen by an enlargement of the scales.

The material undergoes a positive expansion from room temperature to about 200°C, followed by a contraction, still in region I, crossing the axis with 0 ppm expansion at 285°C. The expansion takes place where most of the physical water is being evaporated. It was observed [2] that the adsorption of water into the porous sol–gel silica dilates the gel structure. The evaporation or desorption of this water should consequently lead to a contraction of the gel structure. This was predicted by West et al. [25] using quantum molecular orbital calculations to study the adsorption of a water molecule onto a fourfold silica ring.

Despite what may appear, the results of this work do not contradict West et al.'s predictions. The presence of adsorbed water in the gel at the beginning of the densification implies a larger average neighbor Si–Si distance in the material, when compared with a porous glass without any adsorbed water. The silicon atoms can be seen in this case trapped in a wider potential well. Heating the sample in this wider potential well causes the material to undergo a larger thermal dilation than it would if no water were present, as is the case of a fully densified sol–gel-derived silica. The coefficient of thermal expansion (CTE) of the silica structure of gels processed at low temperatures is quite high owing to the presence of physisorbed water. The dilation in the beginning of the heating schedule also indicates that densification mechanisms for the sol–gel-derived porous silica are not very pronounced in this temperature range.

4.2. Region II

Region II of densification begins at about 300°C, with other densification mechanisms starting to take place more effectively, and the shrinkage rate increasing. The weight loss in this region is attributed both to removal of water due to the polycondensation reaction and to oxidation of the organic groups present in the material [8]. A linear shrinkage of approximately 8% occurs during this region, from a total linear shrinkage of around 28% at the end of the densification process.

The oxidation of the organic groups cannot be associated with any shrinkage, as it occurs between 350 and 600°C, causing a relatively large increase in the rate of weight loss (Fig. 6) with no correspondent increase in the shrinkage rate (Fig. 1). Consequently, the most probable shrinkage mechanisms in this region are structural relaxation, the polycondensation reaction and classical sintering mechanisms, where structural units rearrange to minimize the surface area.

The contribution of the structural densification to the linear shrinkage of the 30 Å gel–silica samples is calculated from the structural density curve (Fig. 4). At the end of Region II, where the structural density reaches its maximum value, the structural densification accounts for 2% of the 8% shrinkage in this region (Fig. 7). This is the total contribution of structural densification to the densification process. The datapoints above 950°C on the expansion calculated from the structural density values in Fig. 7 cannot be considered, as one cannot separate the masking effect of the pore closure, as explained earlier in this text.

The polycondensation reaction apparently does not promote any appreciable shrinkage during the densification of the dried porous gel. Table 1 shows the number of siloxane bonds formed during each of

the four weight loss stages, as a percentage of the total number of possible siloxane bonds. For the calculation of the total number of possible siloxane bonds, all terminations of the TMOS molecules initially present in the mixture were considered to form ≡Si–O–Si≡. Some contraction could also be caused by dehydration of the silica surface, with a resulting increase in surface energy, but complete dehydration would only cause a 0.13% shrinkage through this mechanism [20].

The total polycondensation estimated to occur for all densification after drying is about 1.036%. Thus, 99% of the polycondensation has already occurred by the end of the drying heat treatment of the gel, below 200°C, and is responsible for all the shrinkage of the gel up to the end of the drying schedule, which is around 14%. This leaves the total contribution of the polycondensation reaction during densification to be only a very small shrinkage of 0.15%. The polycondensation during densification can be followed by the evolution of the FTIR 1122 cm^{-1} asymmetric ≡Si–O–Si≡ stretching vibration peak position with temperature (Fig. 5) which changes very little in region II.

Therefore, sintering has to be the mechanism by which at least 6% of the 8% linear shrinkage in region II occurs. The reason for sintering mechanisms acting at such low temperatures for pure silica is the decrease in the material's viscosity due to the presence of hydroxyls, as reported by other authors [9,11]. Fig. 8 shows dilatometry curves for samples of the 30 Å sol–gel-derived pure silica densified under identical heating schedules, in different atmospheres. Ambient air in this case represents a relative humidity of 55–70%, by contrast with a relative humidity of 0% in the helium and oxygen atmospheres. The −30 000 ppm linear shrinkage depicted corresponds to a 3% shrinkage undoubtedly related to the presence of water in the system, and consequently to a decrease in the viscosity of the material. Low-temperature sintering still occurs in the helium and oxygen atmospheres, because of the water initially present in the system. However, the temperature required for full density is increased and the rate of sintering is decreased in the water-free environments.

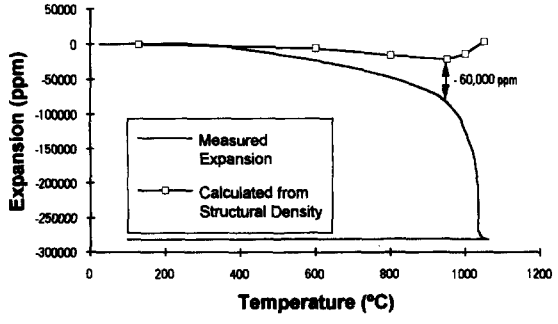

Fig. 7. Expansion of a 30 Å porous silica glass as calculated from the structural density data, superimposed to the dilatometry curve from Fig. 1.

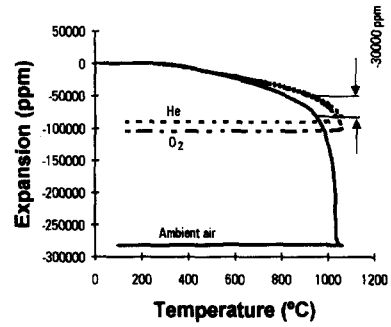

Fig. 8. Dilatometry curve of 30 Å porous silica glasses densified at a heating rate of 15°C/h in three different atmospheres. The difference in shrinkage caused by the absence of water molecules in the helium and oxygen atmospheres is outlined.

4.3. Region III

Around 950°C region III starts (Fig. 1), as indicated by an abrupt increase in the shrinkage rate of the material, with practically no associated weight loss. A 20% linear shrinkage occurs in this region, corresponding to 3/4 of the total shrinkage of the gel. The absence of any significant weight loss (Fig. 6) or increase in the structural density of the material in this region (Fig. 4), implies that sintering is occurring.

Constant-heating-rate techniques were used to model the sintering behavior of the 30 Å porous silica matrices in this region. Isothermal studies can not be related to the initial portion of the sintering reaction, because the most rapid shrinkage takes place while thermal equilibrium is being established [26]. Further, the rapid initial heating necessary for

isothermal studies generates high internal stresses, which often lead to cracking. A constant heating rate is also a better approximation of industrial processing, and the conclusions from such studies can be related to the properties of a glass densified by a practical thermal treatment.

Young and co-workers [26,27] studied the kinetics of initial-stage sintering through constant-heating-rate experiments for the two-sphere geometry and the sintering mechanisms of viscous flow, volume diffusion and boundary diffusion. Bannister [28] studied how the geometry of a particular system affects the parameters of initial stage sintering equations. An equation that describes constant-heating-rate sintering regardless of a prior knowledge of the geometry of the system or of the sintering mechanism was developed by Woolfrey and Bannister [29], which gives the non-isothermal shrinkage rate as a function of Q, the activation energy of the rate-controlling mechanism, and n, a geometry factor

$$(\Delta l/l_0)^{n+1} = \left[\frac{K_0 RT^2(n+1)}{aQ}\right] \exp\left(\frac{-Q}{RT}\right), \quad (1)$$

where $a = \mathrm{d}T/\mathrm{d}t$, the heating rate, is kept constant, Q and n are taken as constants with time at a given temperature, and considering $Q \gg RT$ as is typical for sintering.

A plot of $(\ln \Delta l/l_0)$ versus $1/T$ gives a straight line of slope $s = -Q/(n+1)R$, calculated to be $s = 16.39 \times 10^3$, for a range of linear shrinkage between 9.8 and 14.3%. The calculations were performed for a heating rate of 15°C/h, between 975 and 1013°C, corresponding to the range in region III in which the plot behaves linearly, consistent with the initial-stage sintering. Between 950 and 975°C, the porous silica is actually undergoing a transition from region II to region III.

The activation energy of the process responsible for sintering can be calculated by the Dorn method [29]. This non-isothermal technique calculates the effect on the shrinkage rate of a small step change in temperature, approximated here by a change $\mathrm{d}T$. The activation energy of the process is given by [29]

$$Q \cong \left(\frac{RT_1T_2}{T_1 - T_2}\right) \ln\left(\frac{V_1}{V_2}\right), \quad (2)$$

where V_1 is the shrinkage rate at the initial temperature, T_1 (K), V_2 is the shrinkage rate at the final temperature after the change, T_2 (K), and R is the gas constant.

A plot of the linear shrinkage of a 30 Å porous silica matrix densified at a heating rate of 15°C/h versus time, between 975 and 1013°C, was fitted to a polynomial of the second degree with all correlation coefficients above 0.99. The first derivative of this polynomial led to a function that describes the shrinkage rate as a function of time. As the heating rate is a constant V, and consequently Q, could be calculated for each temperature.

The values of the activation energy, Q, as calculated from Eq. (2), and of n, as calculated from the substitution of the value of Q in Eq. (1), presented large variations because of fluctuations in the heating rate observed during the process. The average geometry factor for this initial sintering stage of the 30 Å porous gel-silicas was found to be $n = 1.0 \pm 0.3$, with an activation energy, $Q = 65 \pm 9$ kcal/mol. For $n = 0.7$, the lower limit of the calculated average, the densification geometry could correspond to the sintering by viscous flow of a cylindrical array, as proposed by Scherer [8,30].

The activation energy around 65 kcal/mol is close to half of the value measured by Hetherington et al. [9] for the viscous flow of a silica glass with 0.12 wt% water. Based on isothermal studies, Scherer et al. [12] found an activation energy for viscous sintering of a silica-based multicomponent sol–gel-derived glass of 122 kcal/mol. In the same study, Scherer et al. also found activation energies as low as 26 kcal/mol for the same system, only considering data from the initial portion of the isothermal holds. The low values were due to the influence of the variation of OH content in the gels with temperature.

An activation energy of 65 kcal/mol for the initial sintering of the 30 Å porous silica glasses indicates that viscous flow is taking place at this early sintering stage, along with dehydroxylation [31]. The geometry of the system may be represented by the cylindrical array model described by Scherer, as indicated by the measured value of the geometry factor, n. These results may be employed empirically to predict the behavior of a particular gel during densification. The reasonable values found validate

the use of constant-heating-rate methods for the analysis of the sintering process of pure silica gels, enabling an easy extrapolation for industrial processing.

5. Conclusions

Densification of sol–gel-derived 30 Å porous silica matrices can be divided into three distinct regions, according to the shrinkage rate and the rate of weight loss in constant heating rate experiments. Region I extends from room temperature to 300°C, and presents a linear expansion of about 0.1% associated with an increased CTE of the pure silica network in the presence of physical water, followed by a contraction of the same amount related to the loss of physically adsorbed water molecules. Region II occurs between 300 and 950°C, with an overall linear shrinkage of approximately 8%, 2% of which is related to the skeletal densification of the material, 0.15% being caused by polycondensation. Sintering mechanisms enhanced by the presence of water molecules are responsible for the remaining contraction. Region III was observed to occur between 950 and 1060°C, with a linear shrinkage of about 20% caused by sintering. The initial sintering, modeled by constant-heating-rate experiments, was found to occur with an apparent activation energy of approximately 65 kcal/mol associated with viscous flow and dehydroxylation.

Financial support from the Brazilian National Council of Research, CNPq, and from the Air Force Office of Scientific Research under Air Force Grant number F49620-92-J-0351 is gratefully acknowledged.

References

[1] L.L. Hench, S.H. Wang and J.L. Noguès, in: Multifunctional Materials, ed. Robert L. Gunshov Vol. 878 (SPIE, Bellingham, WA, 1988) p. 76.
[2] L.L. Hench and J.K. West, Chem. 90 (1990) 33.
[3] L.L. Hench, F.G. Araujo, J.K. West and G.P. LaTorre, J. Sol–Gel Sci. Technol. 2 (1994) 647.
[4] F.G. Araujo, T. Chia and L.L. Hench, J. Sol–Gel Sci. Technol. 2 (1994) 729.
[5] L.L. Hench, J.K. West, B.F. Zu and R. Ochoa, in: Gel-Silica Hybrid Optics, SPIE, San Diego, CA, July 8–13, 1990, vol. 1328, p. 230.
[6] D. Avnir, D. Levy and R. Reisfeld, J. Phys. Chem. 88 (1984), 5956.
[7] G.F. Erickson, in: Proc. Int. Conf. on Lasers, Lake Tahoe, Dec. 7–11, 1987 (STS, McLean, VA, 1987) p. 338.
[8] C.J. Brinker, G.W. Scherer and E.P. Roth, J. Non-Cryst. Solids 72 (1985) 345.
[9] G. Hetherington, K.H. Jack and J.C. Kennedy, Phys. Chem. Glasses 5 [5] (1964). 130.
[10] G.J. Roberts and J.P. Roberts, Phys. Chem. Glasses 5 [1] (1964). 137.
[11] J.M. Jewell, M.S. Spess and J.E. Shelby, J. Am. Ceram. Soc. 73 (1990) 132.
[12] G.W. Scherer, C.J. Brinker and E.P. Roth, J. Non-Cryst. Solids 72 (1985) 369.
[13] J.K. West and L.L. Hench, J. Mater. Sci. 29 (1994) 3601.
[14] J.K. West, J. Kunetz, F.G. Araujo and L.L. Hench, in: Sol–Gel Optics III, ed. J.D. Mackenzie, San Diego, CA (1994) p. 724.
[15] J.H. de Boer, The Structure and Properties of Porous Materials (Butterworth, London, 1958) p. 68.
[16] S. Lowell, Introduction to Powder Surface Area (Wiley, New York, 1979) p. 63.
[17] A.J. Hunt, in: Chemical Processing of Advanced Materials, ed. L.L. Hench and J.K. West (Wiley, New York, 1992) p. 341.
[18] G.W. Scherer, J. Am. Ceram. Soc. 67 (1984) 709.
[19] G.W. Scherer, J. Am. Ceram. Soc. 60 (1977) 243.
[20] C.J. Brinker and G.W. Scherer, Sol–Gel Science (Academic Press, New York, 1990) p. 675.
[21] C.T. Kirk, Phys. Rev. B38 (1988) 1255.
[22] T. Chia, PhD dissertation, University of Florida (1992).
[23] T. Chia, L.L. Hench, C. Qin and C.K. Hsieh, J. Appl. Opt. 33 (1994) 3486.
[24] W.L. Vasconcelos, PhD dissertation, University of Florida (1989).
[25] J.K. West, B.F. Zhu, Y.C. Cheng and L.L. Hench, J. Non-Cryst. Solids 121 (1990), 51.
[26] W.S. Young and I.B. Cutler, J. Am. Ceram. Soc. 53 (1970) 659.
[27] W.S. Young, S.T. Rasmussen and I.B. Cutler, in: Ultra-Fine Grain Ceramics, ed. J.J. Burke, N.L. Reed and V. Weiss (Syracuse University, Syracuse, NY, 1970) p. 185.
[28] M.J. Bannister, J. Am. Ceram. Soc. 51 (1968) 548.
[29] J.L. Woolfrey and M.J. Bannister, J. Am. Ceram. Soc. 55 (1972) 390.
[30] G.W. Scherer, J. Am. Ceram. Soc. 60 (1977) 236.
[31] J.K. West and S. Wallace, in: Chemical Processing of Advanced Materials, ed. L.L. Hench and J.K. West (Wiley, New York, 1992) p. 159.